Journal of Power Sources 196 (2011) 8234–8240

Contents lists available at ScienceDirect

Journal of Power Sources

journal homepage: www.elsevier.com/locate/jpowsour

# Mechanical durability of proton exchange membranes with catalyst platinum dispersion

Ruiliang Jia[a,b], Binghong Han[b], Kemal Levi[b], Takuya Hasegawa[c], Jiping Ye[d], Reinhold H. Dauskardt[b,*]

[a] Department of Mechanical Engineering, Stanford University, Stanford, CA 94305, USA
[b] Department of Materials Science and Engineering, Stanford University, 496 Lomita Mall, Durand Bldg., Room 121, Stanford, CA 94305-2205, USA
[c] Nissan Research Center, Nissan Motor Co., Ltd., 1 Natsushima-cho, Yokosuka 237-8523, Japan
[d] Research Department, Nissan ARC LTD., 1 Natsushima-cho, Yokosuka 237-0061, Japan

ARTICLE INFO

*Article history:*
Received 15 April 2011
Received in revised form 25 May 2011
Accepted 25 May 2011
Available online 1 June 2011

*Keywords:*
Proton exchange membrane
Fuel cell
platinum
Bulge test
Tearing test
Nafion®

ABSTRACT

The durability of proton exchange membrane (PEM) fuel cells remains a challenging issue for their long term operational use. Degradation of the PEM related to dissolution of the adjacent catalyst and re-deposition into the PEM significantly reduces cell efficiency. We investigate the effects of platinum (Pt) dispersions intended to simulate the re-deposited catalyst on the mechanical durability of the PEM. The bulge technique was applied to characterize the mechanical properties of PEMs simulating pressure loading on fully hydrated membranes in fuel cells. The results showed that with increasing Pt dispersion concentration the stiffness of the PEMs increased, and the membranes became less ductile and inclined to fracture at lower stresses under pressure loading. We also used the out-of-plane tearing test to characterize membrane fracture behavior which revealed the harmful effects of Pt dispersion on the fracture resistance under different environmental conditions. Deterioration in fracture resistance was explained in terms of the Pt distribution and aggregation as defects inside the membranes as characterized by electron microscopy. Fracture was shown to initiate preferentially at the interface of Pt particles and the polymer matrix, and propagate through the defect regions in polymer with lower energy, thus reducing the overall fracture resistance of the PEM.



## 1. Introduction

Proton exchange membrane fuel cells (PEMFCs) are a promising power source in stationary, portable, and automotive applications [1–3]. Despite significant improvements in efficiency of these fuel cells in recent years, the durability of current PEMFCs is still a challenging issue for their practical use [4]. In particular, degradation of proton exchange membranes (PEMs), including chemical decomposition induced by a hydrogen peroxide byproduct [5–12] and mechanical damage of the membranes under pressure loading [13–20], represents common failure modes that limit the lifetime of fuel cells.

The performance of PEMFCs is also significantly dependent on the electrocatalytic activity of catalysts such as platinum (Pt) and Pt alloys in both electrodes [21]. The deleterious effect of catalyst degradation on fuel cells efficiency has been investigated [22–25], and the phenomenon of Pt dissolution in the adjacent catalyst layer and subsequent re-deposition into the PEM after long-term operation was also reported [26]. On the other hand, it has also been reported that Pt dispersions in PEMs suppress chemical degradation of the molecular structure of the membranes [27]. Notwithstanding such observation, however, the effects of such Pt dispersions on the mechanical durability of PEMs are currently unknown.

Accordingly, in this study we investigated the mechanical properties of PEMs with Pt dispersions intended to simulate the effect of re-deposited Pt catalyst. The bulge testing method was applied to simulate pressurized loading on hydrated membranes in fuel cells. This method was previously used with a gas pressure medium to characterize PEMs' strength and resistance to gas leakage [17–19], and was also applied to analyze the effect of foreign cation contamination on the mechanical reliability of hydrated PEMs using water as a pressure medium [20]. Here we studied not only the biaxial stress–strain behavior of the PEM-Pt with various Pt concentrations, but also their fracture toughness under hydrated pressure loading. The results showed that with increasing Pt dispersion concentration the stiffness of the membranes increased. Pt dispersion also made the membranes less ductile and inclined to fracture at lower stresses. In addition, we used the tearing test to characterize the out-of-plane fracture behavior of PEM-Pt. Pt dispersions had

*Abbreviations:* PEM, proton exchange membrane; PFSA, perfluorosulfonic acid; DIW, distilled water.

* Corresponding author. Tel.: +1 650 725 0679; fax: +1 650 725 4034.
*E-mail addresses:* dauskardt@stanford.edu, rhd@stanford.edu (R.H. Dauskardt).

0378-7753/$ – see front matter © 2011 Elsevier B.V. All rights reserved.
doi:10.1016/j.jpowsour.2011.05.069

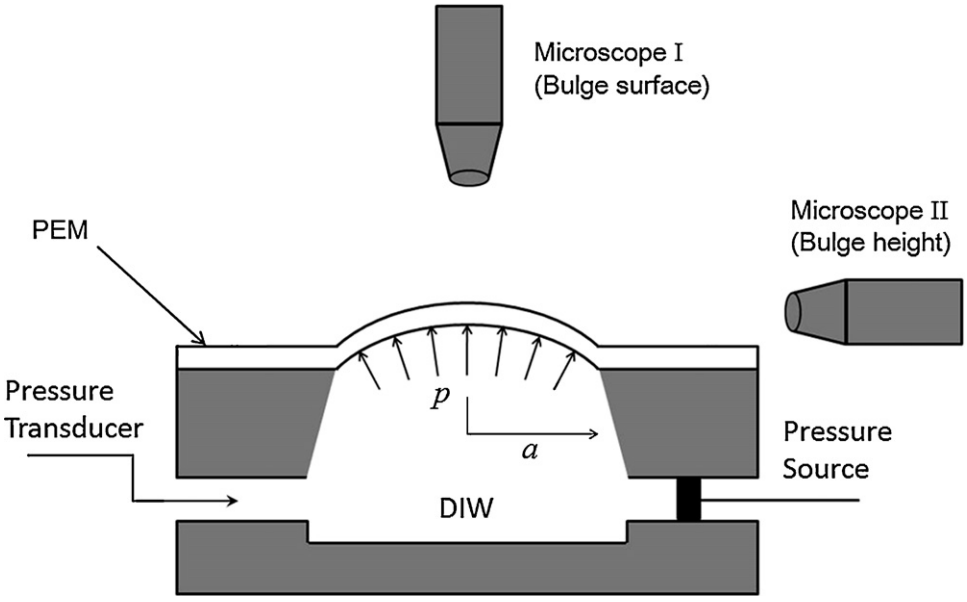


**Fig. 1.** Schematic diagram of the bulge test apparatus.

deleterious effects on the fracture resistance of the membranes under different environmental conditions and was explained in terms of the Pt distribution and aggregation inside the membranes as characterized by electron microscopy. Fracture was shown to initiate at the interface of Pt particles and the polymer matrix, and propagate through the defect regions in polymer with lower energy, thus reducing the overall fracture resistance of PEM. The deterioration in mechanical property and fracture toughness of the membranes indicated that catalyst Pt dissolution and subsequent re-deposition may be implicated in the acceleration of mechanical degradation of PEMs, which is detrimental for the overall durability of a fuel cell.

## 2. Experimental

### 2.1. Membranes preparation

Nafion® perfluorosulfonic acid (PFSA) polymers were used as a representative material. There were several methods to incorporate Pt into Nafion® membranes [28–30]. In this study, the PEM-Pt samples were prepared by dispersing the designed amounts of Pt powders (platinum black, fuel cell grade, ≥99.9% trace metals basis, Sigma–Aldrich®, Inc.) into a PFSA polymer solution (5 wt% Nafion® 117 solution, Sigma–Aldrich®, Inc.), and the various Pt/dry PFSA mass ratios were adjusted to be in a range of 1–75%, respectively. A homogeneous suspension of the mixtures was created with bath sonication for 2 h, and then immediately cast onto a flat glass surface, which was heated at 60 °C until the solvent was completely removed by evaporation. Pure PEMs were also prepared using a 5 wt% Nafion® solution with the same casting and evaporating procedures.

The membranes were removed from the glass surface, and then were treated with a 3 wt% $H_2O_2$ solution for 1 h to oxide organic impurities, followed by 0.5 M $H_2SO_4$ aqueous solution at 23 °C for 1 h to remove ionic impurities [31]. Next, we rinsed the membranes in distilled water (DIW) to remove the excess acid, and wiped them with filter paper. Finally, the membranes were dried at 30 °C for 24 h before use. The membrane thickness was determined by the volume of solution cast per unit area. The resulting thickness of each specimen was measured with a digital micrometer (Digimatic Micrometer, Mitutoyo Corporation, Japan) prior to the experiments and were all 50 ± 10 μm.

### 2.2. Characterization of platinum

The catalyst Pt dispersed inside the membranes was examined by transmission electron microscopy (TEM). Cross-sectional specimens for TEM observation were prepared by ultramicrotomy. A small piece of the membrane was first embedded in a 2.3 M sucrose solution and frozen in liquid $N_2$. Then the membrane was sectioned by a cryo-ultramicrotome (Leica ULTRACUT UCT) using a glass knife at −80 °C. The sectioned films with an approximate thickness of 80 nm were attached on a TEM copper grid (SPI Supplies® 300 Mesh, West Chester, PA). The TEM observations (FEI Tecnai G2 F20 X-TWIN with EDS) were conducted at a 200 kV operating voltage. The tearing test fracture surface of PEM-Pt specimens was observed with a Hitachi S-3400N variable pressure scanning electron microscope (VP-SEM) (Hitachi Ltd., Pleasanton, CA) operated at 15 kV and 40 Pa, with a working distance of 7–8 mm.

### 2.3. Bulge test

Detailed information of our bulge test technique, including experimental apparatus, testing procedures and data analysis, has been described previously [20], and is only briefly reviewed here.

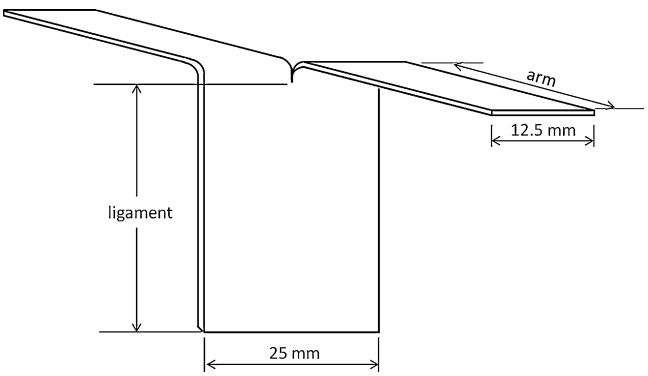


**Fig. 2.** Out-of-plane tearing test specimen.

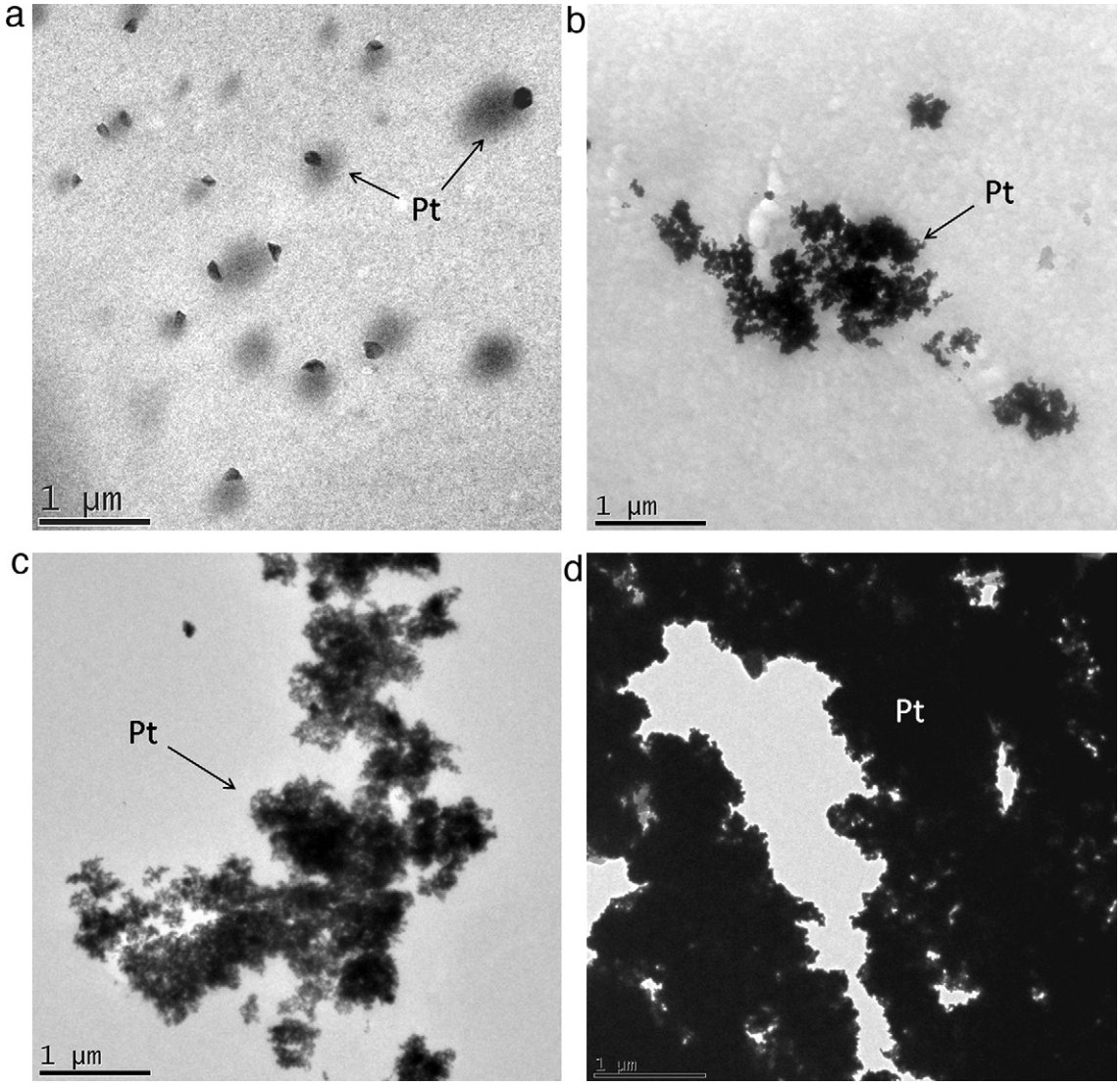


**Fig. 3.** TEM images of PEM-Pt with Pt/PFSA mass ratios of (a) 1%, (b) 5%, (c) 10% and (d) 70%.

Bulge testing was conducted using a plexiglass unit encasing a drilled cavity with two channels, which were filled with DIW as the pressure medium (Fig. 1). PEM-Pt specimens (15 mm × 15 mm) were first clamped onto the orifice of the cavity, and one side of the membrane was exposed to DIW for 10 min to achieve the fully hydrated condition before testing. Then the specimens were pressurized with the DIW to form a balloon like shape at a constant medium flow rate of 0.089 μL $s^{-1}$, and the pressure inside the system was measured by a pressure transducer. During the experiments, one microscope was used to measure the bulge height of the specimens, and another one was positioned vertically above the bulge system to monitor the surface of the bulged membrane for penetration of the DIW. The bulge test experiments were carried out at a constant temperature and relative humidity condition, i.e., at 23 °C and 25% RH.

To determine the biaxial stress and strain in the PEM, the pressurized membrane was modeled as a section of a thin-walled spherical pressure vessel having uniform equal biaxial stress and curvature. Then, the equal biaxial stress, $\sigma$, in the membranes is given by:

$$\sigma = \frac{pR}{2t} \tag{1}$$

where $p$ is the applied pressure, $R$ is the radius of the sphere and t is thickness of the tissue. Using the Pythagorean Theorem, the radius of pressure orifice, $a$, and bulge height, $h$, was related to $R$:

$$R = \frac{h}{2} + \frac{a^2}{2h} \tag{2}$$

The bulge height $h$ of the PEM specimens was measured with optical microscopy from the side view by focusing on the highest center of bulged specimens.

The thickness of the bulged membrane was calculated assuming constant volume deformation with the equation:

$$t = \frac{t_0}{\lambda^2} \tag{3}$$

where $t_0$ is the initial, strain-free thickness of the PEM measured before clamping on the test system, and $\lambda$ is the biaxial stretch given by:

$$\lambda = \frac{L}{2a} \tag{4}$$

where $L$ is the length of the arc of the bulge. The biaxial true strain, $\varepsilon$, was obtained from the biaxial stretch using:

$$\varepsilon = \ln(\lambda) \tag{5}$$

The biaxial modulus $B$ of the membrane was determined from the initial slope of stress–strain curves before the onset of non-linear yield loading.

### 2.4. Out-of-plane tearing test

Out-of-plane tearing test (trouser test) specimens were prepared by cutting PEM-Pt samples to have two legs with an identical width of 12.5 mm and an untorn ligament length of ~22 mm, as shown in Fig. 2. The tests were conducted with a high precision mechanical test system (Delaminator Adhesion Test system, DTS Company, Menlo Park, CA) under two environmental conditions of 25% and 100% RH at 23 °C inside an environmental chamber (Associated Environmental System, Inc., Ayer, MA). The legs were clamped in the testing machine and loaded in tension in opposite directions at a constant displacement rate of 100 $\mu m\,s^{-1}$. An out of plane fracture propagated in the ligament. The tearing fracture energy was calculated using [32]:

$$G_{tear} = \frac{2F}{t} \quad (6)$$

where $F$ is the average tearing force during fracture propagation and $t$ is the thickness of the membrane. For each type of PEM-Pt with a specific Pt concentration, three specimens were tested, and the average values of $G_{tear}$ were reported.

## 3. Results and discussion

### 3.1. Characterization of platinum dispersed in PEMs

TEM images of the PEM-Pt with different Pt/PFSA mass ratios are shown in Fig. 3. The PEM with 1% Pt was characterized by relatively uniformly distributed Pt particles (dark spots), but with increasing Pt/PFSA mass ratio the Pt particles tend to aggregate into larger clusters with complex shapes. The phenomenon of Pt particles redeposition and aggregation in PEMs from catalyst layers after fuel cell operation has been reported [26,33–35]. It was shown that the relatively larger Pt clusters (with maximum sizes of ~500 nm) were mainly distributed near the electrodes and smaller particles (with diameters less than 50 nm) were scattered further from the catalyst layers. The PEM-Pt specimens analyzed in this study therefore are representatives of both regions in PEMs with re-deposited catalyst after fuel cell operation. In subsequent sections we rationalize the mechanical behavior in terms of these Pt dispersions.

### 3.2. Bulge test on PEMs with Pt dispersion

The pressure applied on PEM-Pt with various Pt/PFSA mass ratios during bulge testing is shown as a function of time in Fig. 4. With increasing Pt concentrations the initial slope of the pressure vs. time curves increased and the membranes burst pressure decreased.

Using the applied pressure and corresponding bulge height measured from the side view microscope (Fig. 1), the biaxial stress and strain of the PEM-Pt with various Pt concentrations were calculated using Eqs. (1)–(5). Fig. 5(a) and (b) shows the biaxial stress–strain curves over the full strain range and the initial strain range (0–0.03), respectively. The biaxial stress–strain curves have a similar shape but the membranes with higher Pt concentration tend to fracture (bulge burst) earlier at lower stress values (Fig. 5(a)), and the biaxial elastic modulus $B$ increased with increasing Pt/PFSA mass ratio (Fig. 5(b)).

The fracture stress of PEM-Pt in bulge tests decreased with increasing Pt/PFSA mass ratios, becoming constant at ~8 MPa, as shown in Fig. 6. This trend represents the deleterious effect of catalyst Pt dispersion on the fracture resistance of PEMs under pressure

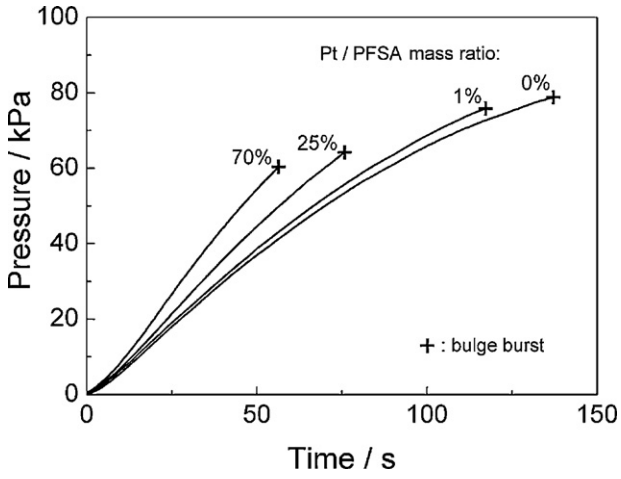


**Fig. 4.** The pressures applied on PEM-Pt with various Pt/PFSA mass ratios as a function of the pressurizing time until bulge burst.

loading. TEM images of PEM-Pt clearly reveal that cracks initiate preferentially at the interface of Pt particles and the polymer matrix (Fig. 7(a)), and cracks were subsequently observed to propagate through a defect region with Pt distribution in the polymer (Fig. 7(b)). Increasing amounts of Pt particles and clusters are therefore expected to result in the reduced fracture stress observed in the bulge tests with increasing Pt/PFSA mass ratio. This result is

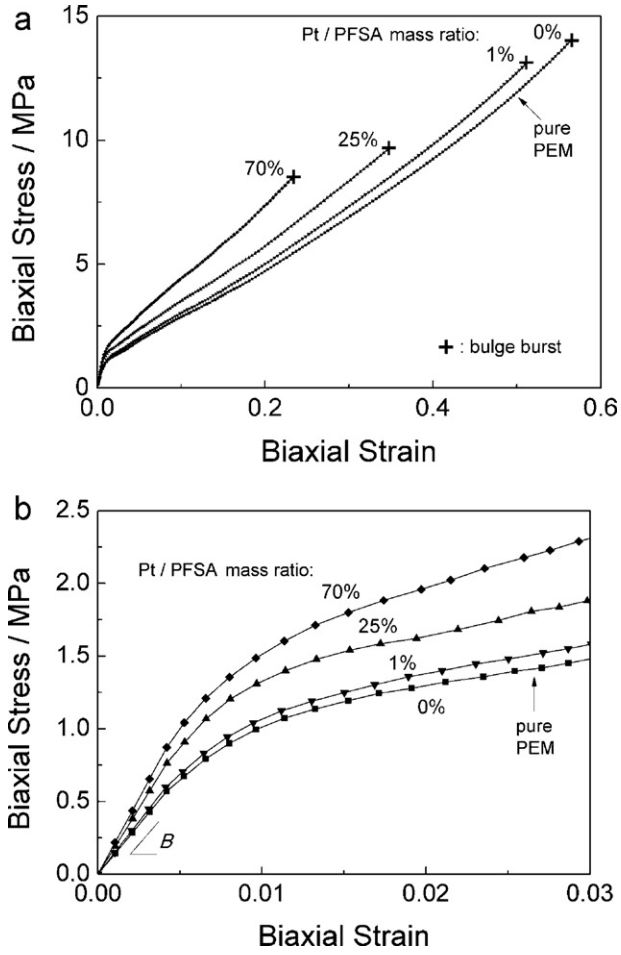


**Fig. 5.** Biaxial stress vs. strain of PEM-Pt with various Pt/PFSA mass ratios (■) 0% (pure PEM); (▼) 1%; (▲) 25%; and (♦) 70%) over (a) full strain range and (b) initial strain range of 0–0.03.

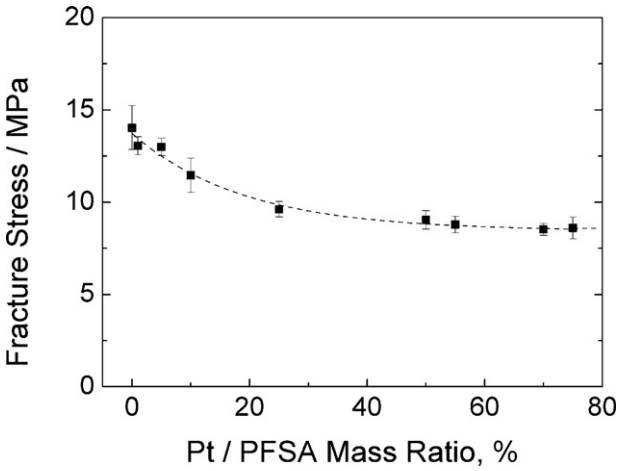


**Fig. 6.** Fracture stress of PEM-Pt as a function of Pt/PFSA mass ratios in bulge test.

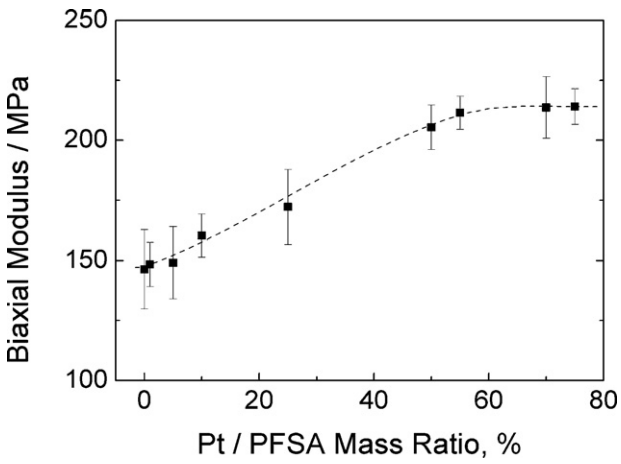


**Fig. 8.** Biaxial modulus of PEM-Pt as a function of Pt/PFSA mass ratios.

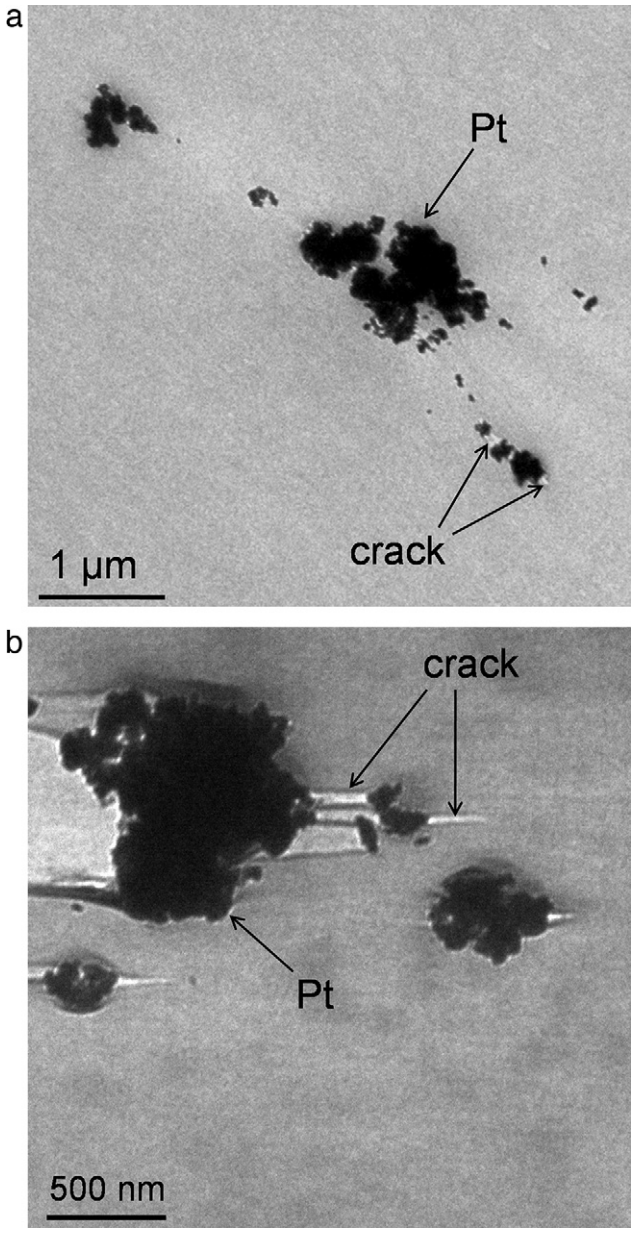


**Fig. 7.** TEM images of PEM-Pt with (a) cracks initiation and (b) cracks propagation.

consistent with an interesting phenomenon recently reported [36]. It was reported that catalyst coated membranes have shorter lifetimes than pure PEMs in blister fatigue tests, suggesting the large amount of Pt depositing on PEM surfaces tends to reduce the mechanical reliability of membranes.

The biaxial moduli $B$ of PEM-Pt are summarized and compared in terms of the Pt/PFSA mass ratios in Fig. 8. It is noticeable that the biaxial modulus gradually increased with increasing Pt concentration, reaching a maximum at a Pt/PFSA mass ratio of ~55%. The incorporation of catalyst Pt particles and clusters therefore had the effect to stiffen the PEMs. However, we note that the resulting stiffness is significantly lower than that of pure Pt bulks (Young's modulus $E$ ~158 GPa) or even plasma deposited Pt nanostructured films ($E$ ~140 GPa) [37], which using effective medium theory would be expected to have a larger effect of increasing the PEM-Pt modulus. For the present membranes, the reduced effect of the Pt dispersions is likely related to the high volume fraction of porosity within the Pt clusters (Fig. 3(d)).

### 3.3. Tearing test on PEMs with Pt dispersion

The forces measured in the PEM-Pt tearing tests were used to calculate the corresponding tearing fracture energy, $G_{tear}$, using Eq. (6). Fig. 9 shows the results of $G_{tear}$ for PEM-Pt with various Pt concentrations, tested at 25% RH and 100% RH.

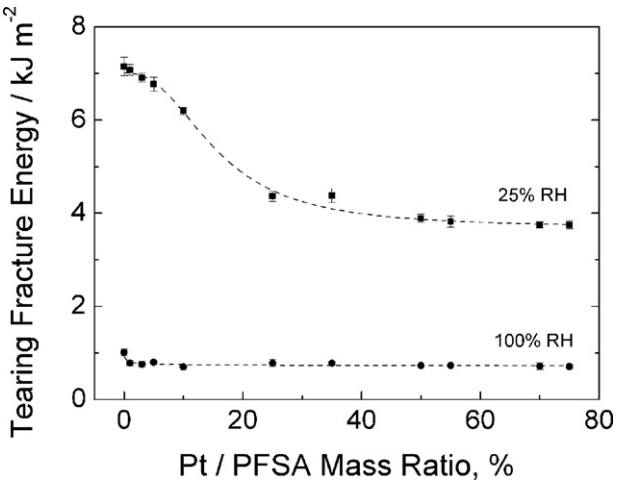


**Fig. 9.** Tearing fracture energy of PEM-Pt as a function of Pt/PFSA mass ratios tested at 25% RH and 100% RH, respectively.

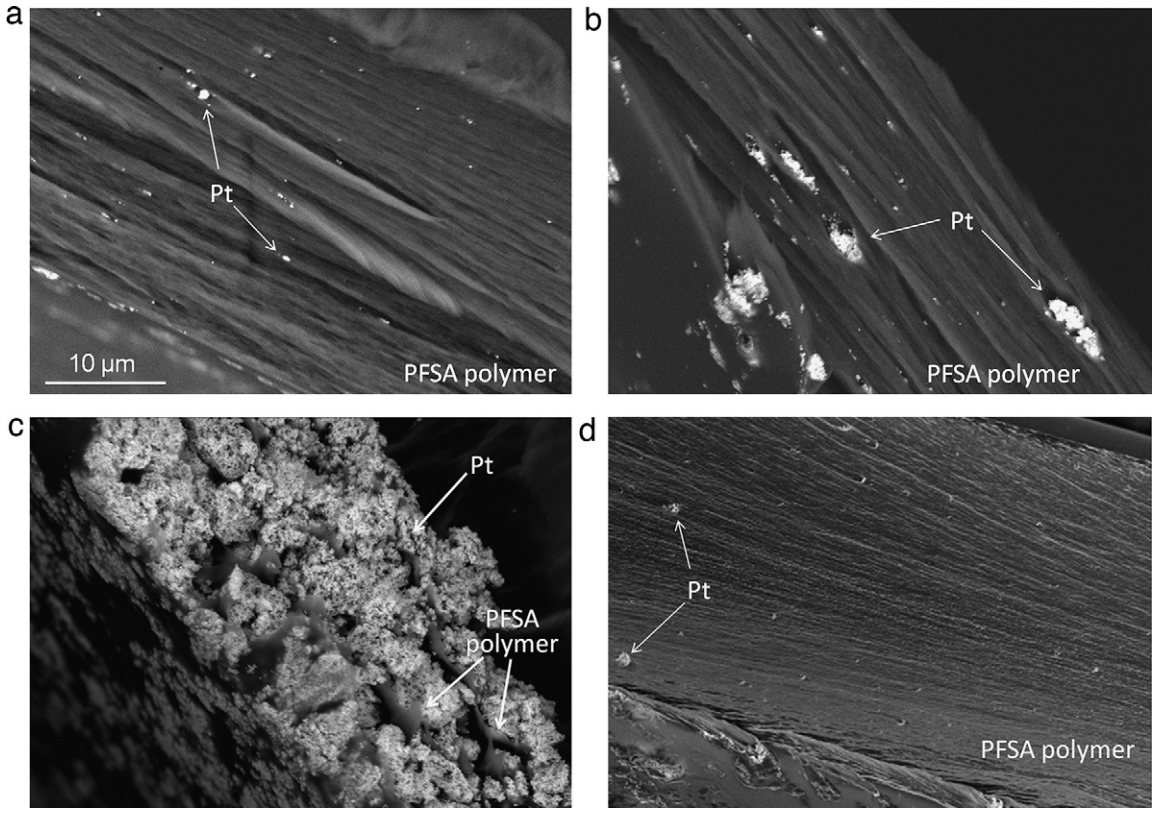


**Fig. 10.** SEM images of tearing fracture surfaces of PEMs with Pt/PFSA mass ratios of (a) 3%, (b) 10% and (c) 70% tested at 25% RH, and (d) 3% tested at 100% RH.

The tearing fracture energy tested at 25% RH was gradually reduced with increasing concentrations of Pt dispersed in the membranes, and became relatively constant after the Pt/PFSA mass ratios were higher than 50%. SEM images of the fracture surfaces of the membranes with selected Pt dispersions are shown in Fig. 10. It can be observed that at a lower Pt concentration (3%) the Pt particles (the largest particles with ~1 μm diameter) were distributed inside the membrane (Fig. 10(a)). As Pt/PFSA mass ratio increased to 10%, larger Pt clusters appeared on the fracture surface (Fig. 10(b)). Similarly to the fracture mechanism of PEM-Pt under pressure loading discussed in the previous section, cracks would initiate easier at the interface of Pt particles and the polymer matrix, and propagate through defect regions with Pt distribution in the polymer, thus reducing the overall fracture resistance of PEM. When the Pt concentration increased further to 70%, we observed a small amount of PFSA polymers existing among Pt with macro porous structures on the fracture surface (Fig. 10(c)), and the corresponding fracture energy was reduced ~40% compared with that of pure PEMs. The relatively constant energy values for the membranes with Pt concentration higher than 50% would probably be related to the significant volume fraction of Pt in the membranes. As the proportion of polymers decreased to a certain level, the fracture resistance of PEM-Pt specimens was mainly dependent on the porous Pt and would not decreased significantly further with increasing Pt/PFSA mass ratio.

It is also noticeable in Fig. 9 that the tearing fracture energy $G_{tear}$ of all PEM-Pt specimens at 100% RH decreased significantly compared to their dry counterparts measured at 25% RH, and was slightly lower than that of pure PEMs measured at 100% RH. SEM images of fracture surfaces of PEM-Pt with the same Pt concentration (3%) but tested at different humidity conditions illustrate noticeably different features, as compared in Fig. 10(a) and (d). The fracture surface of the membranes tested at 25% RH had feather-like structures, but the surface of the membrane fractured at 100% RH showed narrow strips along the fracture propagation direction, which represented a common feature of brittle materials. The deleterious effect of water absorption on the mechanical durability of PEMs has been previously reported [20]. The decreased fracture resistance under hydrated condition was explained by the presence of excessive water that can not only weakens the ionic interaction in clusters formed by sulfonic acid groups, but also reduces the intermolecular forces of the main chains in the PFSA polymers [38,39]. Therefore the significant decrease in fracture energy of PEM-Pt under fully hydrated conditions is related to the combined effects of water absorption and the role of the Pt dispersions discussed above.

## 4. Conclusion

In this research, we studied the effect of Pt dispersions intended to simulate the re-deposited catalyst on the mechanical durability of PEMs with thin film characterization approaches. The bulge testing was applied to assess the biaxial mechanical behavior of membranes by using water as a medium to simulate hydrated pressurized loading on PEMs in fuel cells. The stiffness of PEM-Pt increased with the increasing Pt concentrations, but the membranes became less ductile and their fracture stresses were noticeably reduced. In addition, we used the out-of-plane tearing test to characterize the fracture properties of PEM-Pt. The results showed that the Pt dispersion had deleterious effects on fracture resistance of the membranes under different environments. These mechanical and fracture behaviors were explained in terms of Pt distribution and aggregation inside the membranes as characterized by electron microscopy. Fracture was shown to

initiate preferentially at the interface of Pt particles and the polymer matrix, and propagate through the Pt defect regions in polymer with lower energy, thus reducing the overall fracture resistance of the PEM. The deterioration in mechanical property and fracture toughness of the membranes indicated that catalyst Pt dissolution and subsequent re-deposition may be implicated in the acceleration of mechanical degradation of PEMs.

## Acknowledgement

The authors would like to thank Dr. John J. Perrino and Dr. Lydia-Marie Joubert from CSIF and Dr. Hui Wu from Materials Sciences and Engineering Department at Stanford University for their help with the electron microscopy experiments.

## References

[1] P. Costamagna, S. Srinivasan, J. Power Sources 102 (2001) 242–252.
[2] C.K. Dyer, J. Power Sources 106 (2002) 31–34.
[3] H. Inaka, S. Sumi, K. Nishizaki, T. Tabata, A. Kataoka, H. Shinkai, J. Power Sources 106 (2002) 60–67.
[4] J. Wu, X.Z. Yuan, J.J. Martin, H. Wang, J. Zhang, J. Shena, S. Wu, W. Merida, J. Power Sources 184 (2008) 104–119.
[5] J. Qiao, M. Saito, K. Hayamizu, T. Okada, J. Electrochem. Soc. 153 (2006) A967–A974.
[6] H. Tang, S. Peikang, S.P. Jiang, F. Wang, M. Pan, J. Power Sources 170 (2007) 85–92.
[7] N. Ramaswamy, N. Hakim, S. Mukerjee, Electrochim. Acta 53 (2008) 3279–3295.
[8] M. Inaba, M. Sugishita, J. Wada, K. Matsuzawa, H. Yamada, A. Tasaka, J. Power Sources 178 (2008) 699–705.
[9] S. Kundu, L.C. Simon, M.W. Fowler, Polym. Degrad. Stab. 93 (2008) 214–224.
[10] A.C. Fernandes, E.A. Ticianelli, J. Power Sources 193 (2009) 547–554.
[11] T. Aoki, A. Matsunaga, Y. Ogami, A. Maekawa, S. Mitsushima, K. Ota, H. Nishikawa, J. Power Sources 195 (2010) 2182–2188.
[12] T. Sugawara, N. Kawashima, T.N. Murakami, J. Power Sources 196 (2011) 2615–2620.
[13] W. Liu, K. Ruth, G. Rusch, J. New Mater. Electrochem. Syst. 4 (2001) 227–232.
[14] X.Y. Huang, R. Solasi, Y. Zou, M. Feshler, K. Reifsnider, D. Condit, S. Burlatsky, T. Madden, J. Polym. Sci. Part B: Polym. Phys. 44 (2006) 2346–2357.
[15] C. Bao, M.G. Ouyang, B.L. Yi, Int. J. Hydrogen Energy 31 (2006) 1879–1896.
[16] A. Collier, H. Wang, X. Zi Yuan, J. Zhang, D.P. Wilkinson, Int. J. Hydrogen Energy 31 (2006) 1838–1854.
[17] D.A. Dillard, Y. Li, J.R. Grohs, S.W. Case, M.W. Ellis, Y.-H. Lai, M.K. Budinski, C.S. Gittleman, J. Fuel Cell Sci. Technol. 6 (2009) 031014–031021.
[18] Y. Li, D.A. Dillard, S.W. Case, M.W. Ellis, Y.-H. Lai, C.S. Gittleman, D.P. Miller, J. Power Sources 194 (2009) 873–879.
[19] J.R. Grohs, Y. Li, D.A. Dillard, S.W. Case, M.W. Ellis, Y.-H. Lai, C.S. Gittleman, J. Power Sources 195 (2010) 527–531.
[20] R. Jia, B. Han, K. Levi, T. Hasegawa, J. Ye, R.H. Dauskardt, J. Power Sources 196 (2011) 3803–3809.
[21] A.S. Arico, S. Srinivasan, V. Antonucci, Fuel Cells 1 (2001) 133.
[22] Y. Shao, G. Yin, Y. Gao, J. Power Sources 171 (2007) 558–566.
[23] M.S. Wilson, F.H. Garzon, K.E. Sickafus, S. Gottesfeld, J. Electrochem. Soc. 140 (1993) 2872–2877.
[24] T.R. Ralph, M.P. Hogarth, Platinum Met. Rev. 46 (2002) 117–135.
[25] T. Patterson, Pre-Print Archive-American Institute of Chemical Engineers, Spring National Meeting, New Orleans, LA, 2002, pp. 313–318.
[26] K. Yasuda, A. Taniguchi, T. Akita, T. Ioroi, Z. Siroma, Phys. Chem. Chem. Phys. 8 (2006) 746–752.
[27] M. Aoki, H. Uchida, M. Watanabe, Electrochem. Commun. 8 (2006) 1509–1513.
[28] E.K.W. Lai, P.D. Beattie, F.P. Orfino, E. Simon, S. Holdcroft, Electrochim. Acta 44 (1999) 2559–2569.
[29] Z. Liu, Z. Qun Tian, S. Ping Jiang, Electrochim. Acta 52 (2006) 1213–1220.
[30] K. Itaya, H. Takahashi, I. Uchida, J. Electroanal. Chem. 208 (1986) 373–382.
[31] M.B. Satterfield, P.W. Majstrik, H. Ota, J.B. Benziger, A.B. Bocarsly, J. Polym. Sci. 44 (2006) 2327–2345.
[32] Y. Li, J.K. Quincy, S.W. Case, M.W. Ellis, D.A. Dillard, Y.-H. Lai, M.K. Budinski, C.S. Gittleman, J. Power Sources 185 (2008) 374–380.
[33] T. Akita, A. Taniguchi, J. Maekawa, Z. Siroma, K. Tanaka, M. Kohyama, K. Yasuda, J. Power Sources 159 (2006) 461–467.
[34] E. Guilminot, A. Corcella, F. Charlot, F. Maillard, M. Chatenet, J. Electrochem. Soc. 154 (2007) B96–B105.
[35] T. Madden, D. Weiss, N. Cipollini, D. Condit, M. Gummalla, S. Burlatsky, V. Atrazhev, J. Electrochem. Soc. 156 (2009) B657–B662.
[36] M.T. Pestrak, Y. Li, S.W. Case, D.A. Dillard, M.W. Ellis, Y.H. Lai, C.S. Gittleman, J. Fuel Cell Sci. Technol. 7 (2010) 0410091–04100910.
[37] M.C. Salvadori, I.G. Brown, A.R. Vaz, L.L. Melo, M. Cattani, Phys. Rev. B 67 (2003) 153404.
[38] Y. Tang, A.M. Karlsson, M.H. Santare, M. Gilbert, S. Cleghorn, W.B. Johnson, J. Mater. Sci. 425 (2006) 297–304.
[39] F. Bauer, S. Denneler, M. Willert-Porada, J. Polym. Sci. Part B: Polym. Phys. 43 (2005) 786–795.